

## Supporting Information

### **Coupled Ion Desolvation and Nucleation Control for Stable Zinc Anodes Enabled by a Polyoxometalate-Crosslinked Nanocellulose Separator**

*Yilin Zhang, Chenyu Wang, Xuan Li, Yuhuan Ye, Fan Chen, Guoli Ding, Zhiguang Guo, Lei Li, Jun Lei, Huadong Huang, Hongli Yang\*, Shengyang Zhou\*, Zhongming Li*

*Yilin Zhang, Chenyu Wang, Xuan Li, Yuhuan Ye, Fan Chen, Guoli Ding, Shengyang Zhou*

College of Materials Science and Engineering, Sichuan University, Chengdu 610065, China

*Zhiguang Guo, Lei Li, Jun Lei, Huadong Huang, Hongli Yang, Zhongming Li*

College of Polymer Science and Engineering, Sichuan University, Chengdu 610065, China

*Zhongming Li*

West China Hospital/West China School of Medicine, Sichuan University, Chengdu 610041, China

*Jun Lei, Huadong Huang, Hongli Yang, Shengyang Zhou, Zhongming Li*

State Key Laboratory of Advanced Polymer Materials, Sichuan University, Chengdu 610065, China

\*E-mail: [shengyang.zhou@scu.edu.cn](mailto:shengyang.zhou@scu.edu.cn); [yang.hongli@scu.edu.cn](mailto:yang.hongli@scu.edu.cn)

## Experimental Section

**Materials.** Phosphomolybdic acid (Macklin, China), carboxymethyl nanocellulose dispersion (solid content of 4.8 mg mL<sup>-1</sup>, RISE Research Institutes of Sweden AB, Sweden), zinc foil (50 μm, Oleggeino, China), copper foil (50 μm, Oleggeino, China), glass fiber separator (200 μm, Oleggeino, China), zinc hydroxide (Zn(OH)<sub>2</sub>, Aladdin, China), zinc sulfate heptahydrate (ZnSO<sub>4</sub>, Aladdin, China), lithium sulfate monohydrate (Li<sub>2</sub>SO<sub>4</sub>·H<sub>2</sub>O, Aladdin, China), lithium manganate (LiMn<sub>2</sub>O<sub>4</sub>, Gelon, China), carbon nanotubes (Sigma Aldrich, Hong Kong, China) were used without further purification. The ultrapure water used in this work was produced by an ultrapure water machine (Shanghai Lichen Instrument Technology Co., Ltd., China).

**Preparation of NC and PC separators.** The NC and PC separators were prepared using a method of solution wet-casting. Before the preparation of separators, phosphomolybdic acid was dissolved in deionized water and then neutralized by dissolving Zn(OH)<sub>2</sub> powder until the pH value reached 7. Then, deionized water was added into nanocellulose aqueous dispersion to achieve a diluted dispersion with a solid content of 1 mg mL<sup>-1</sup>. This homogenized diluted dispersion (40 mL) was then mixed with the phosphomolybdic zinc solution (50 μL, 2 mg mL<sup>-1</sup>), followed by an ultrasonic treatment to achieve a homogeneous solution and remove bubbles. This homogeneous solution was cast in a petri dish and placed in a vacuum oven to further degas. It was then left in the oven at 50 °C overnight for drying and finally obtaining the freestanding PC separator. The NC separator was prepared using the same procedures but without the addition of the phosphomolybdic zinc solution.

**Materials Characterization.** The transmission electron microscopy (TEM) images were collected by Tecnai G2 F20 S-TWIN (FEI, U.S.A.). Scanning electron microscopy (SEM) images and energy dispersive spectrometer (EDS) mapping images were collected by using Nova NanoSEM 450 (FEI, U.S.A.). The X-ray diffractometer (XRD) profiles were collected by using a diffractometer with Cu K $\alpha$  radiation (DX-2700B, Dandong Haoyuan Instruments Co., Ltd., China). The wettability properties of separators were tested by a contact angle measurement device (Kruss DSA30S). The X-ray photoelectron spectra (XPS) was recorded on an Axis ultra DLD. The mechanical properties were tested by a universal test machine (Instron 5967, U.S.A.). The Zeta potential data were measured by using a Zeta potential analyzer (Malvern, Zetasizer Nano ZS, U.K.). Fourier-transform infrared spectroscopy (FTIR) spectra were collected by using an infrared spectrometer (Nicolet 6700, Thermal Scientific, U.S.A.). Small angle X-ray scattering (SAXS) patterns were obtained by using a scatter-meter (Xeuss 3.0, France), the SAXS data were fitted by using the following model:<sup>1</sup>

$$I(q) = \frac{A}{q^n} + B \exp\left(-\frac{q^2 r_g^2}{3}\right) + C$$

This model is a two-stage model, where the first term is a power law with a *Porod* exponent  $n$ , which depicts the complexity of the network. The second term is a Guinier form assigned to the size of voids in the radius of gyration  $r_g$ , which are attributed to the water clusters in the entangled nanocellulose network due to water swelling of separators.

**Molecular Dynamics Simulation.** Molecular dynamics simulations were performed

using Materials Studio 2020 software. Before the calculation, we first built two molecular dynamics models. System 1: the molar ratio of water with zinc sulfate was set as 55:2 (5500 water molecules and 200 zinc sulfate molecules). System 2: the molar ratio of water with zinc sulfate and phosphomolybdic was set as 55:2:0.01 (5500 water molecules, 200 zinc sulfate molecules, and 1 phosphomolybdic nanoparticle). Both models are filled and combined according to the molecular ratio. We used the “*Forcite-Dynamics*” module to perform molecular dynamics simulation on the constructed model to explore the diffusion behavior of water molecules in the ionomer. For the molecular dynamic simulation, “*Ultra-fine*” was selected for the calculation quality, “*Dreiding*” was selected for the force field, *Smart* was selected for the algorithm, the “*Nose*” was selected for the thermostat, the temperature was maintained at 298 K, the pressure was maintained at 0 MPa, “*NPT*” was selected for the ensemble, “*Atom based*” and “*Ewald*” were selected for the electrostatic force and van der Waals force, respectively, and the simulation time was set to 1000 ps. We selected each frame of the trajectory file obtained from the molecular dynamic simulation, calculated the radial distribution function of water molecules and zinc ions, and selected the appropriate viewing angle to export the images.

**Zn||Cu Asymmetric Cells Characterization.** The Zn and Cu foil were firstly cut into discs with a diameter of 12 mm. Zn||Cu cells were assembled using CR2032 coin-type cells with 80  $\mu$ L 2 M ZnSO<sub>4</sub> electrolyte at ambient temperature. All the electrochemical tests for Zn||Cu asymmetric cells including the cyclic voltammetry (CV) (potential window: -0.2 V - 0.5 V, scanning rate: 1 mV s<sup>-1</sup>), chronoamperometry (CA) (bias

potential:  $\pm 150$  mV), and chronopotentiometry (CP) (current density:  $1 \text{ mA cm}^{-1}$ ), were performed by using an electrochemical workstation (CHI660E, CH Instruments, U.S.A.). Long-time charging-discharging curves and corresponding Coulomb efficiency were tested by using a battery testing system (Neware, CT-4008, China). The diffusion coefficient of zinc ions ( $D$ ) was measured by using Zn||Cu cells with different separators. At different scan rates, CV curves were obtained at the same potential windows. The value of  $D$  can be calculated by the following equation:

$$I_p = 0.4463nFAC_x V^{1/2} \sqrt{\frac{nFD_x}{RT}}$$

where  $I_p$  is the peak current,  $n$  is the number of electrons gained and lost in the electrode reaction,  $F$  is the Faraday constant,  $A$  is the contact area between electrode plate and electrode solution,  $C_x$  is the concentration of the zinc ions,  $V$  is the scanning rate.

**Zn||Zn Symmetric Cells Characterization.** The assembly procedures of Zn||Zn symmetric cells were same with the Zn||Cu cells as described above. The electrochemical tests for Zn||Zn symmetric cells including the cyclic voltammetry (CV), electrochemical impedance spectroscopy (EIS), and Tafel plots (potential window:  $-0.2 \text{ V} - 0.2 \text{ V}$ , scanning rate:  $1 \text{ mV s}^{-1}$ ) were implemented by using the same electrochemical workstation (CHI660E, CH Instruments, U.S.A.). Zinc ions transfer numbers ( $t_{Zn^{2+}}$ ) of different separators were measured by assembling Zn||Zn symmetric cells based on the following equation:

$$t_{Zn^{2+}} = \frac{I_S(\Delta V - I_0 R_0)}{I_0(\Delta V - I_S R_S)}$$

where  $\Delta V$  is the constant polarization voltage,  $I_0$  and  $I_S$  are the initial current and the

steady-state current based on CA test, respectively.  $R_0$  and  $R_s$  are the initial resistance and the stable resistance based on EIS test, respectively. The Arrhenius activation energy ( $E_a$ ) of the electrolytes within different separators were measured using Zn||Zn cells at different temperature. The  $E_a$  can be calculated by the following equation:

$$\frac{1}{R_{ct}} = A \exp\left(\frac{-E_a}{RT}\right)$$

where  $R_{ct}$  is the resistance obtained from the EIS spectra,  $R$  is the gas constant, and  $T$  is the thermodynamic temperature. *Damköhler* number ( $D_a$ ) can be obtained by the following equation:<sup>2</sup>

$$D_a = \frac{i_0}{i_l}$$

$i_0$  is the exchange current at the electrode which is obtained from GCD curves,  $i_l$  is the diffusion-limited current in the electrolyte which is calculated from:

$$i_l = \frac{4FCD_+}{L}$$

$F$  is the Faraday constant,  $C$  is the salt concentration in the electrolyte solution,  $D_+$  is the cation diffusion coefficient, and  $L$  is the space between physically separated electrodes. *Wagner* number ( $W_a$ ) can be obtained by the following equation:<sup>3</sup>

$$W_a = \frac{R_{ct}}{R_\Omega}$$

$R_{ct}$  is the charge transfer resistance from the EIS spectra and  $R_\Omega$  electrolyte resistance from the EIS spectra.

**Ionic Conductivity Measurements.** The ionic conductivities ( $\sigma$ ) of the electrolytes within different separators were measured by sandwiching the electrolyte-wetted separator with two stainless-steel electrodes. The  $\sigma$  can be calculated by the following equation<sup>4</sup>:

$$\sigma = \frac{L}{RS}$$

where  $L$  is the thickness of the separator,  $R$  is the bulk resistance obtained from EIS test, and  $S$  is the contact area between the separator and the electrode.

**Full Battery Performance Test.** The cathode used in this work was fabricated by mixing carbon nanotubes with  $\text{LiMn}_2\text{O}_4$  particles by using nanocellulose as the binder. The mass ratio of  $\text{LiMn}_2\text{O}_4$ , carbon nanotubes, and nanocellulose was set as 8:1:1. First, all those materials were dispersed in a mixed solution of water and alcohol (1:1), and then sonicated for 15 minutes to make a uniform solution. Following, the mixed solution was vacuum-filtrated and dried overnight at 60 °C. The active mass loading of  $\text{LiMn}_2\text{O}_4$  is 1.5 mg  $\text{cm}^{-2}$ . The full batteries were also assembled using CR2032 coin-type cells with 80  $\mu\text{L}$  electrolyte (2 M  $\text{ZnSO}_4$  + 1 M  $\text{Li}_2\text{SO}_4$ ) at ambient temperature. All the battery performance tests and data processing procedures in this work were performed by using a battery testing system (Neware, CT-4008, China).

## Supplementary Figures and Tables

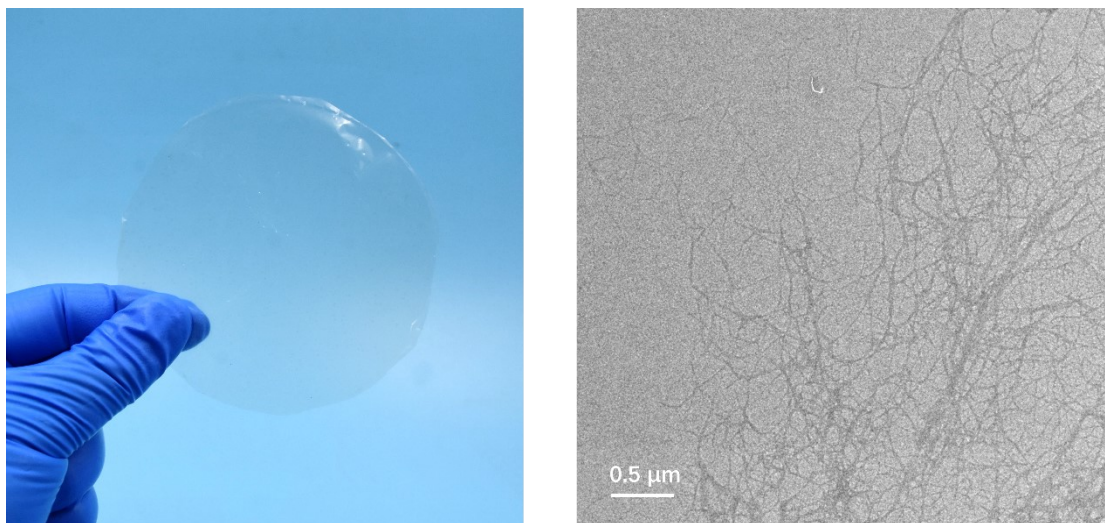


**Figure S1.** Digital photo of a piece of freestanding NC separator and corresponding TEM image of pristine nanocellulose.

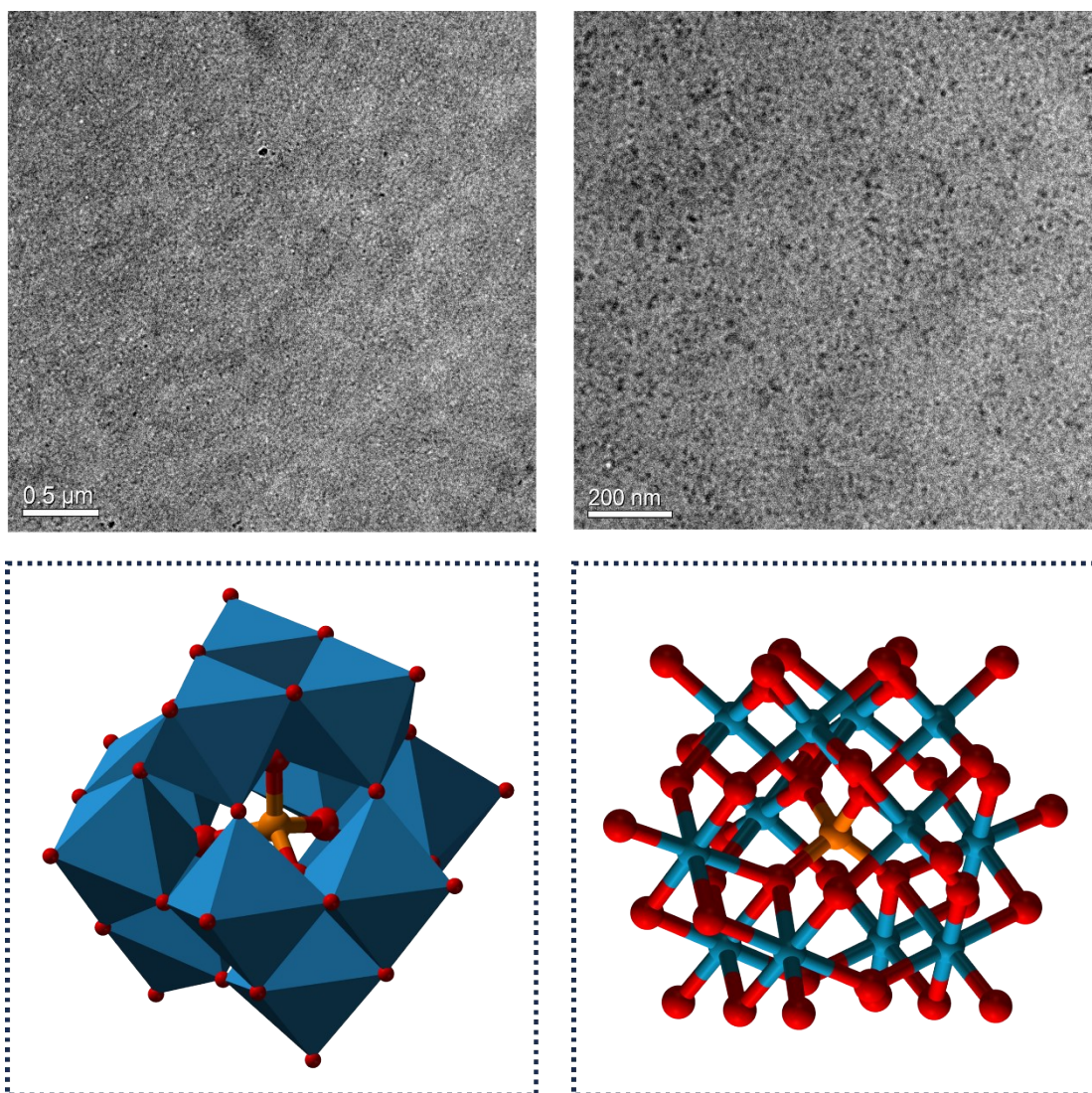


**Figure S2.** TEM images with different magnifications and standard crystal structures of phosphomolybdic studied in this work.

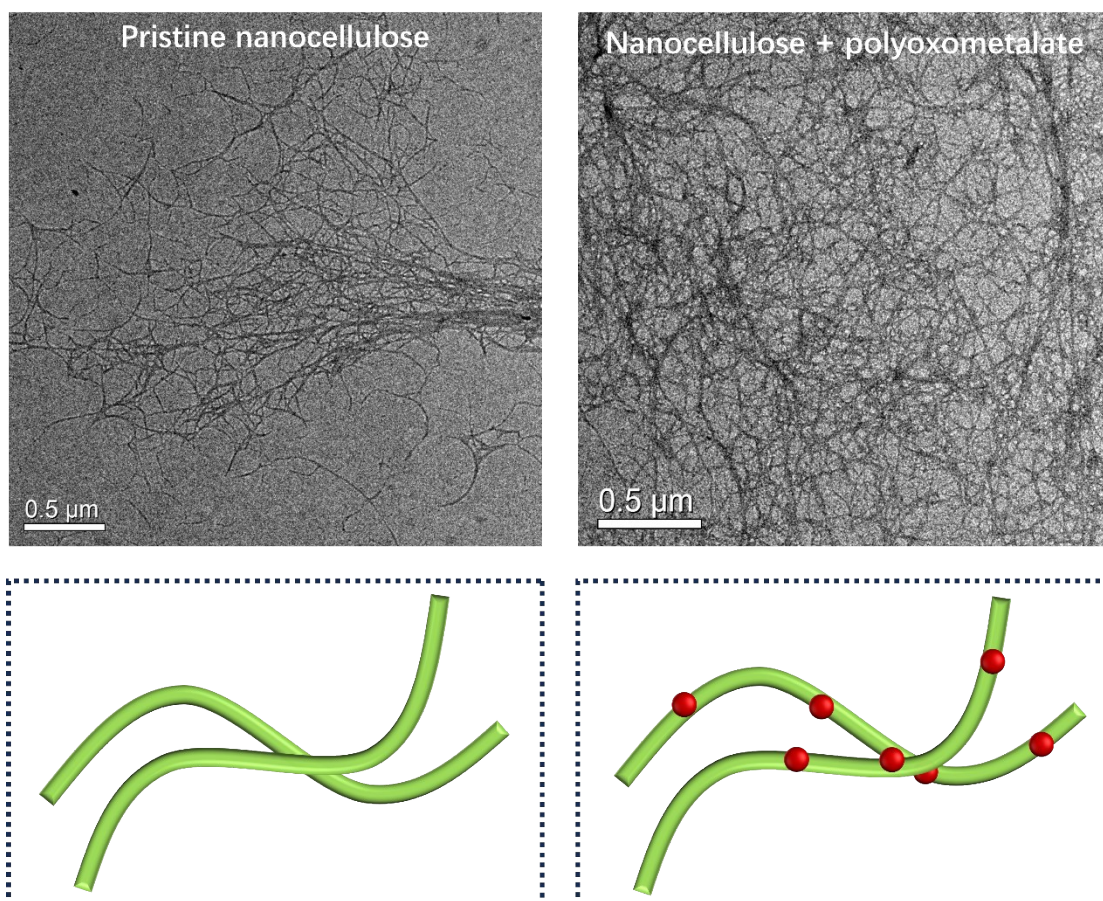


**Figure S3.** TEM images and corresponding morphology schematics of pristine nanocellulose and phosphomolybdic cross-linked nanocellulose networks.

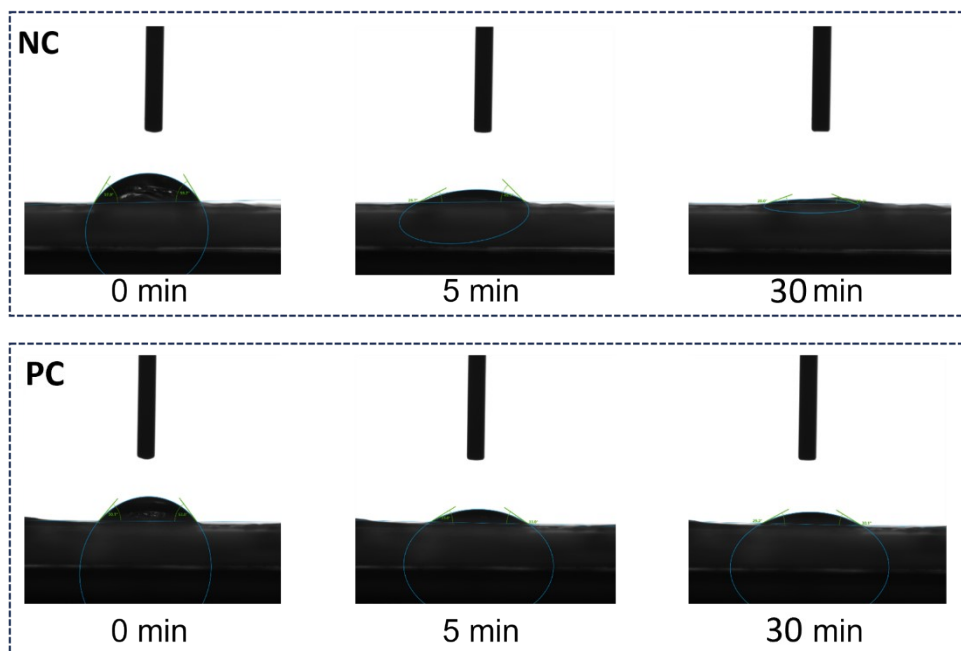


**Figure S4.** Evolution of water contact angles on NC and PC separators over time, indicating differences in hydrophilicity and water absorption behavior.

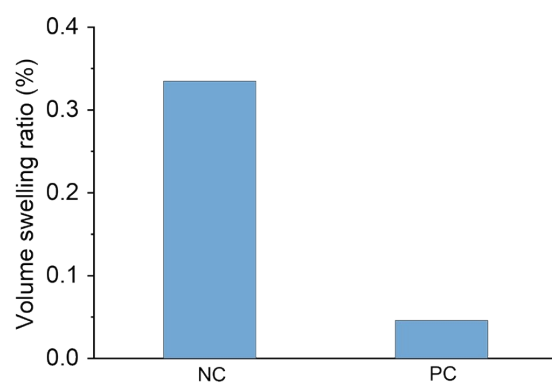


**Figure S5.** Volumetric swelling ratios of NC and PC separators measured after immersion in electrolyte.

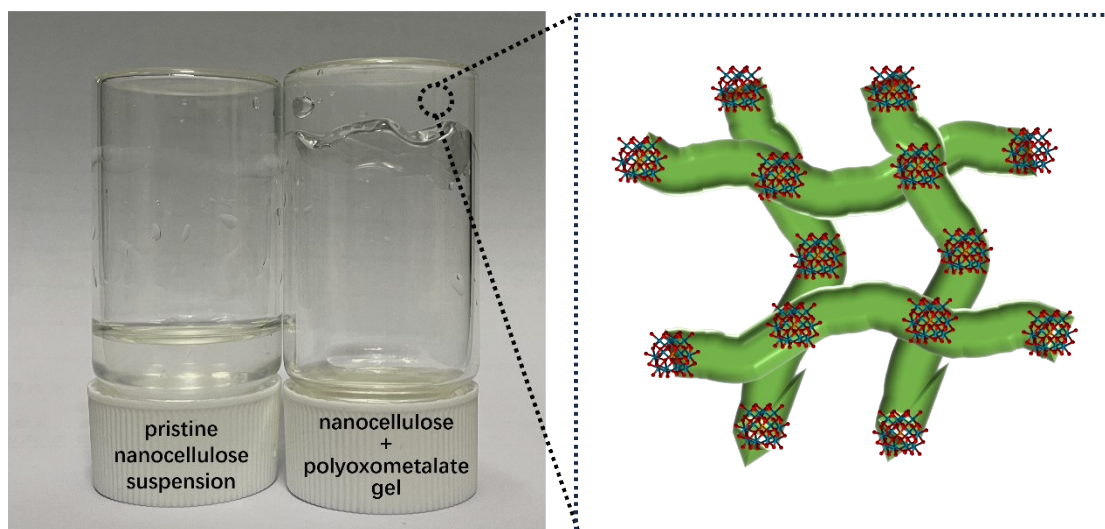


**Figure S6.** Digital photo of diluted pristine nanocellulose aqueous suspension and nanocellulose gel crosslinked by phosphomolybdic. The schematic diagram shows the possible cross-linking structure of nanocellulose with phosphomolybdic nanoparticles.

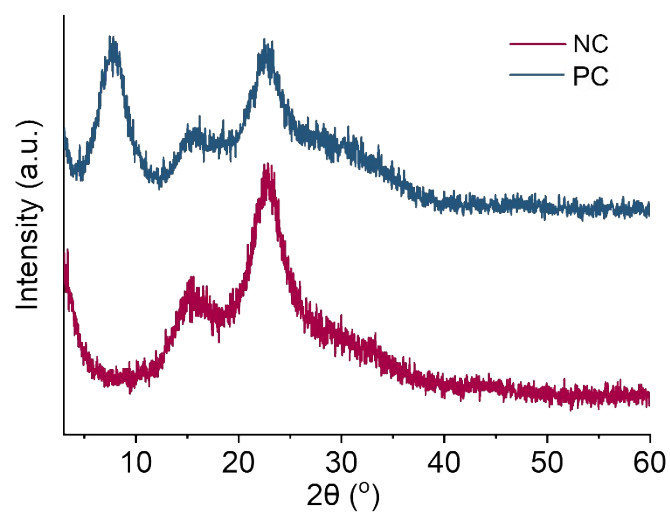
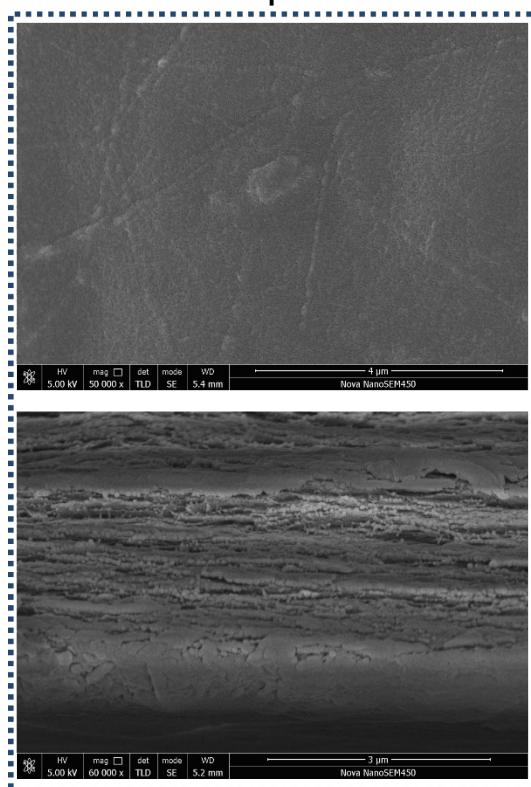


**Figure S7.** XRD profiles of pristine NC separator and PC separators. An additional peak ( $2\theta = 8.5^\circ$ ) can be clearly recognized in the XRD curve of PC, which can attribute to the (001) plane of phosphomolybdic.

NC separator



PC separator

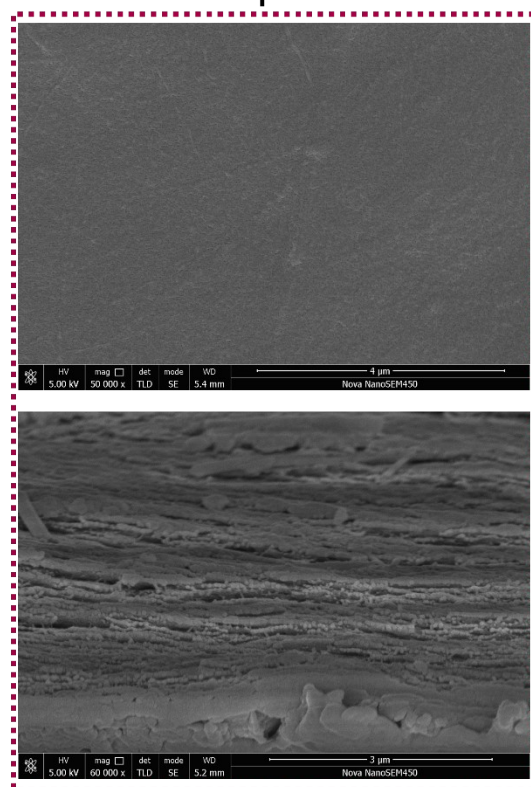


**Figure S8.** Surface and side-view SEM images of NC and PC separators.

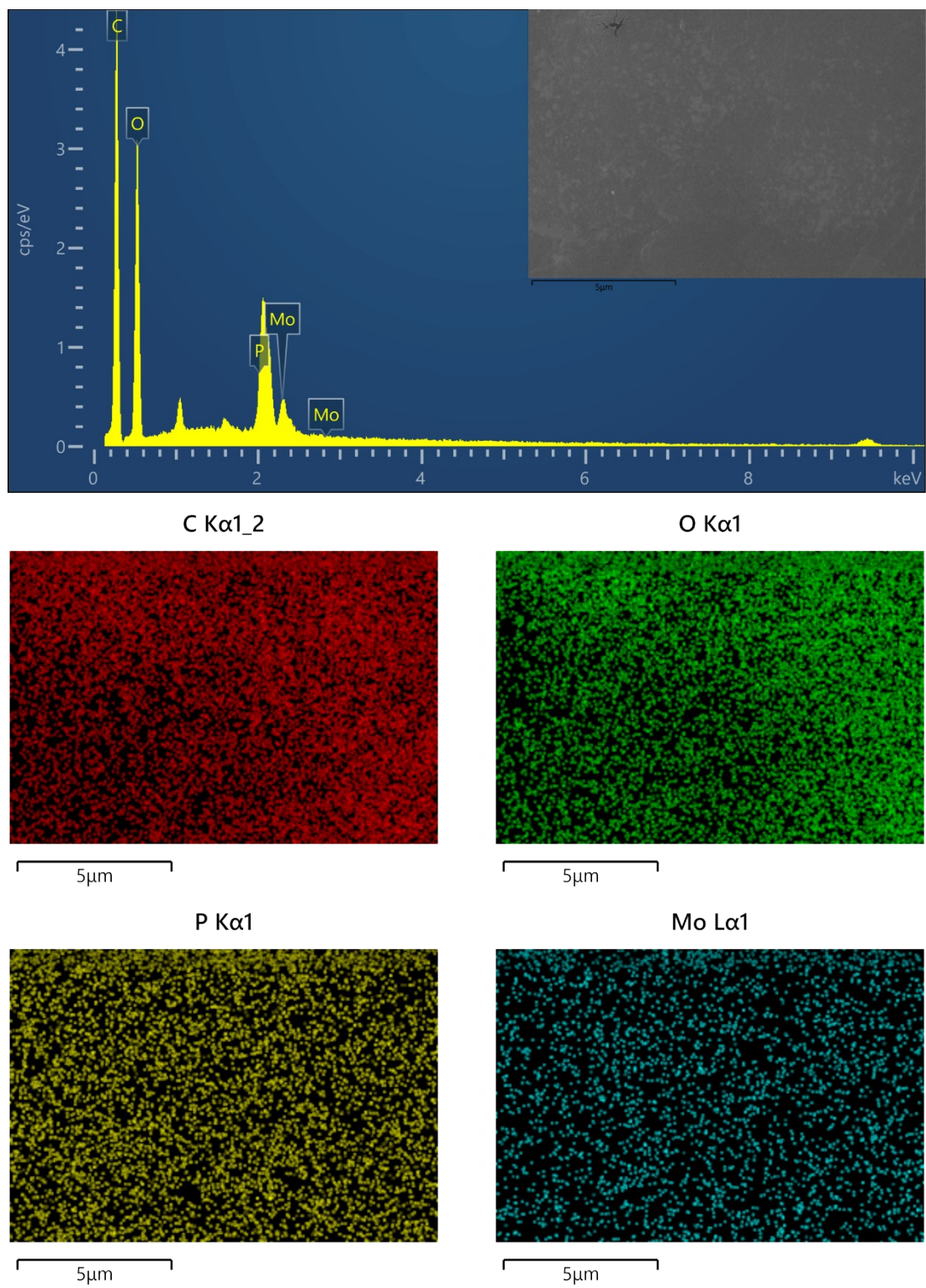


**Figure S9.** EDS spectrum and corresponding mapping images of PC separators.

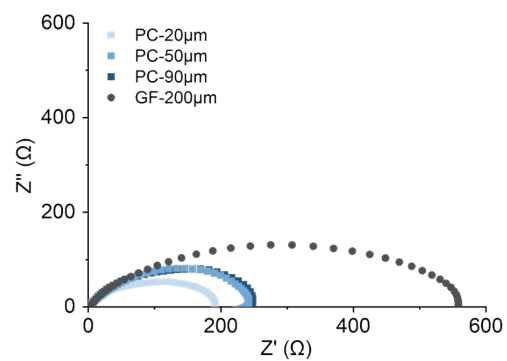


**Figure S10.** Electrochemical impedance spectra of PC separators with varying thicknesses compared to a commercial glass fiber separator.

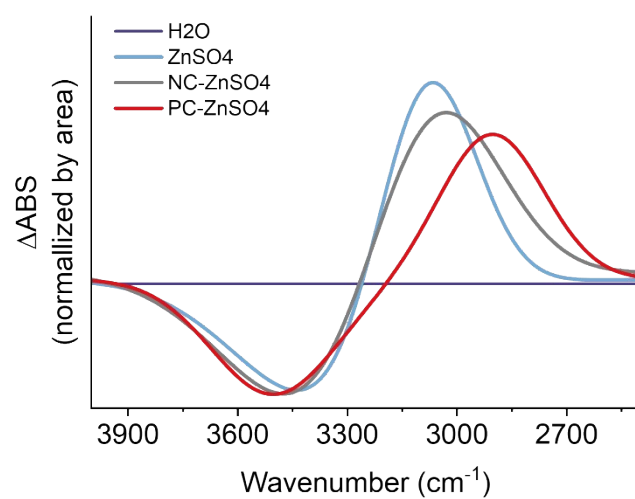


**Figure S11.** Differential ATR-FTIR spectra electrolytes in different separators.

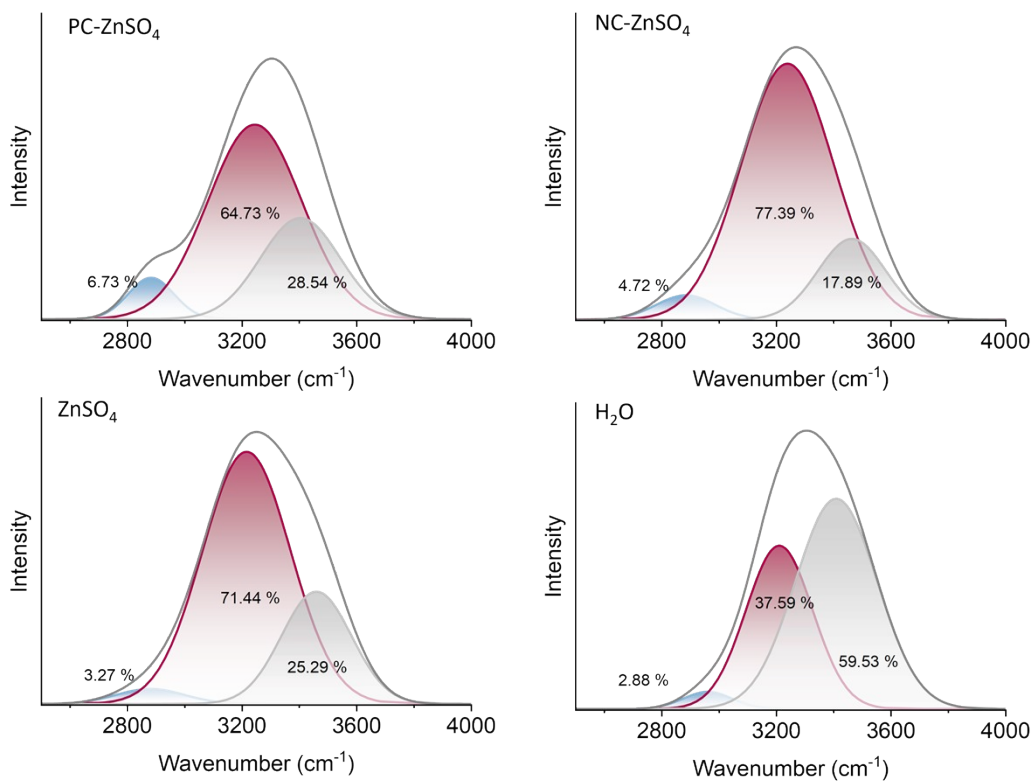


**Figure S12.** ATR-FTIR spectra of hydrogen bonds with peak deconvolution to distinguish different water coordination states.

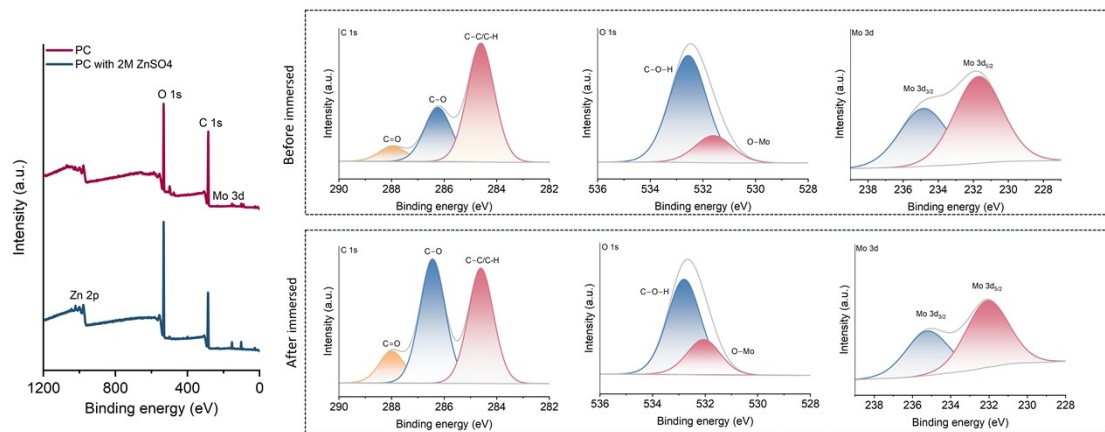


**Figure S13.** X-ray photoelectron spectroscopy (XPS) of the PC separator before and after immersed in electrolyte, including survey spectrum, C 1s, O 1s, and Mo 3d spectra.

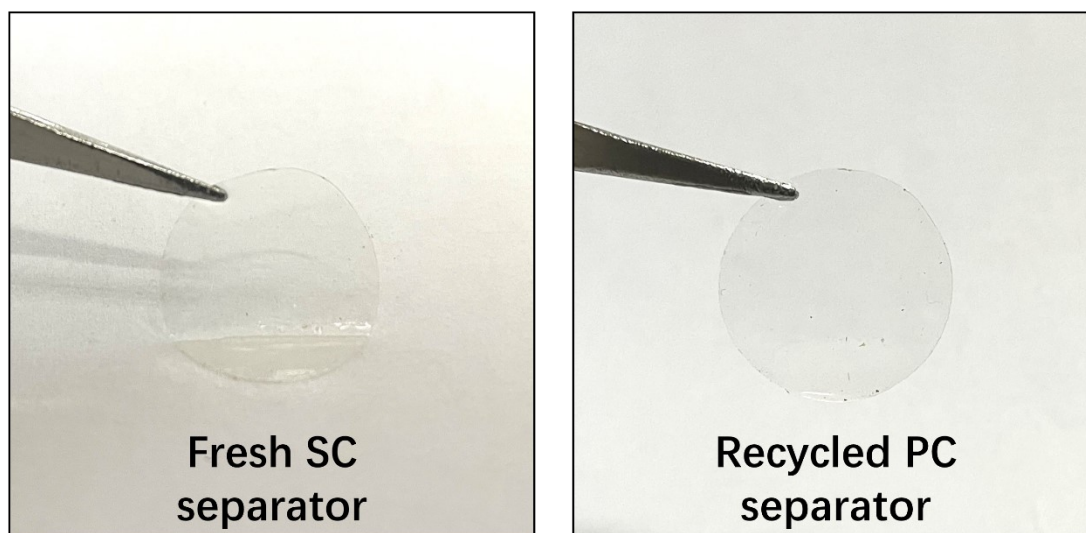


**Figure S14.** Digital photos of PC separators before and after testing in a battery, suggesting the good structural and dimensional stability.

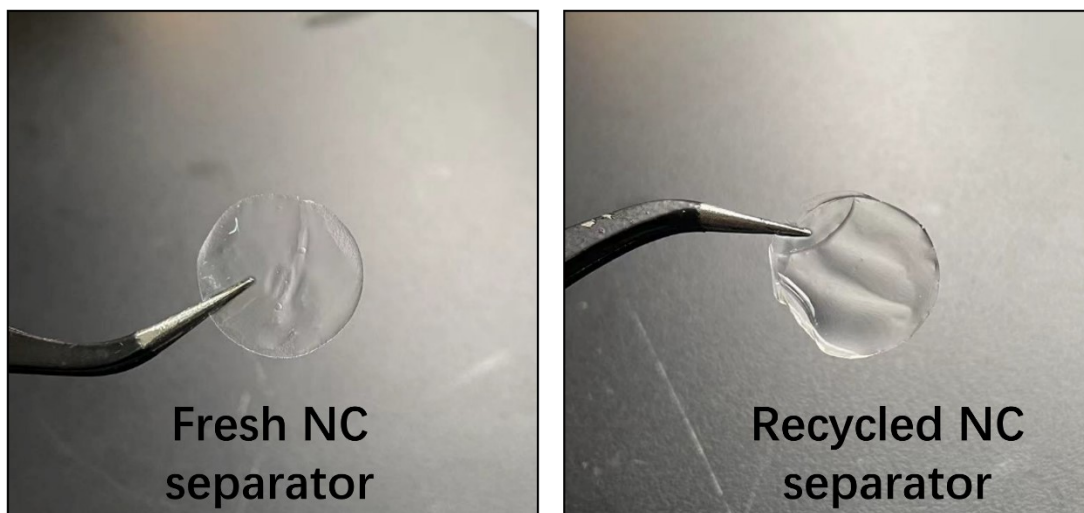


**Figure S15.** Digital photos of NC separators before and after testing in a battery, showing the swelling and dimensional deformation.

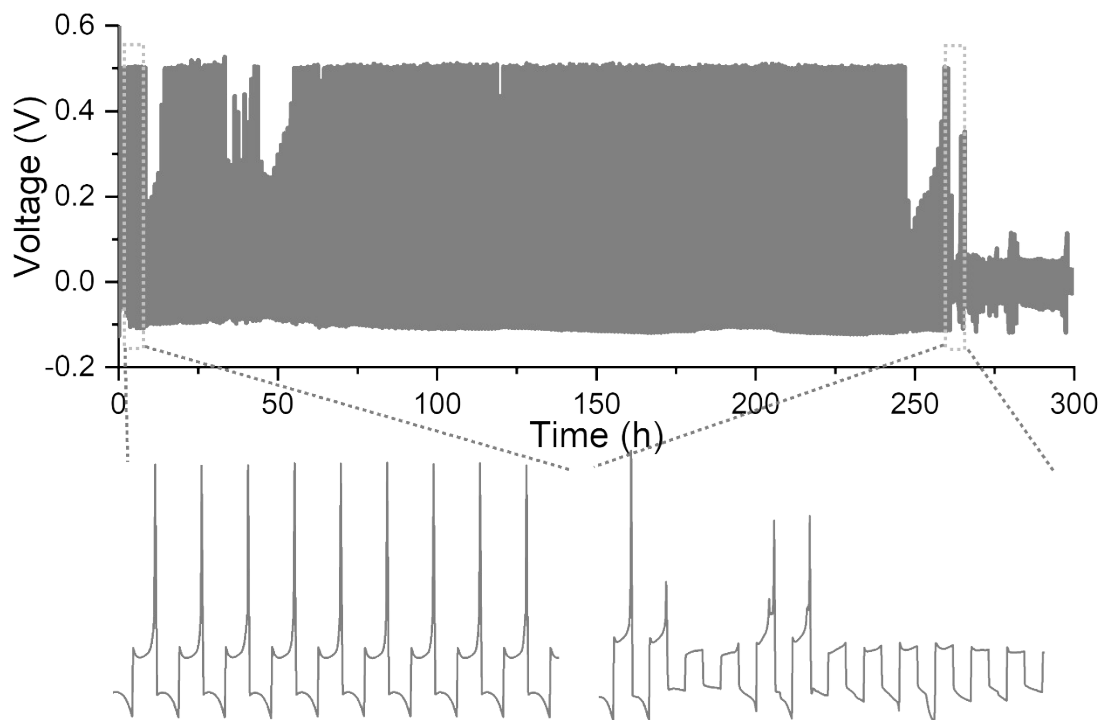


**Figure S16.** Charge-discharge curves of Zn||GF||Cu cell and areal magnification curves at initial and final stages.

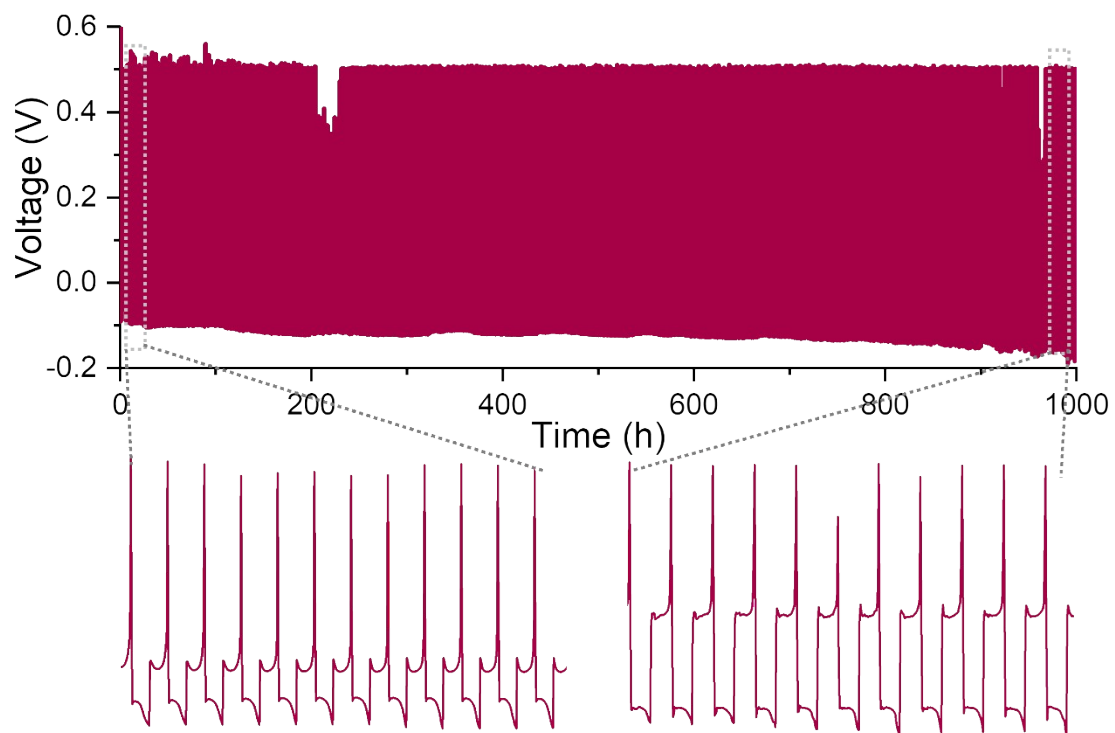


**Figure S17.** Charge-discharge curves of Zn||NC||Cu cell and areal magnification curves at initial and final stages.

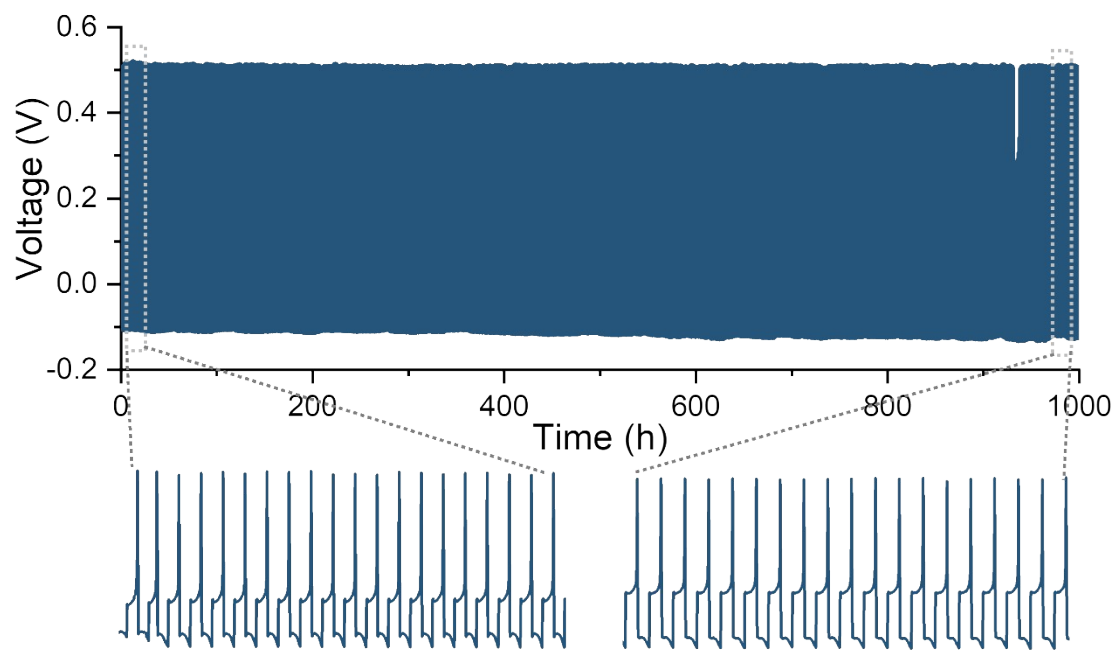


**Figure S18.** Charge-discharge curves of Zn||PC||Cu cell and areal magnification curves at initial and final stages.

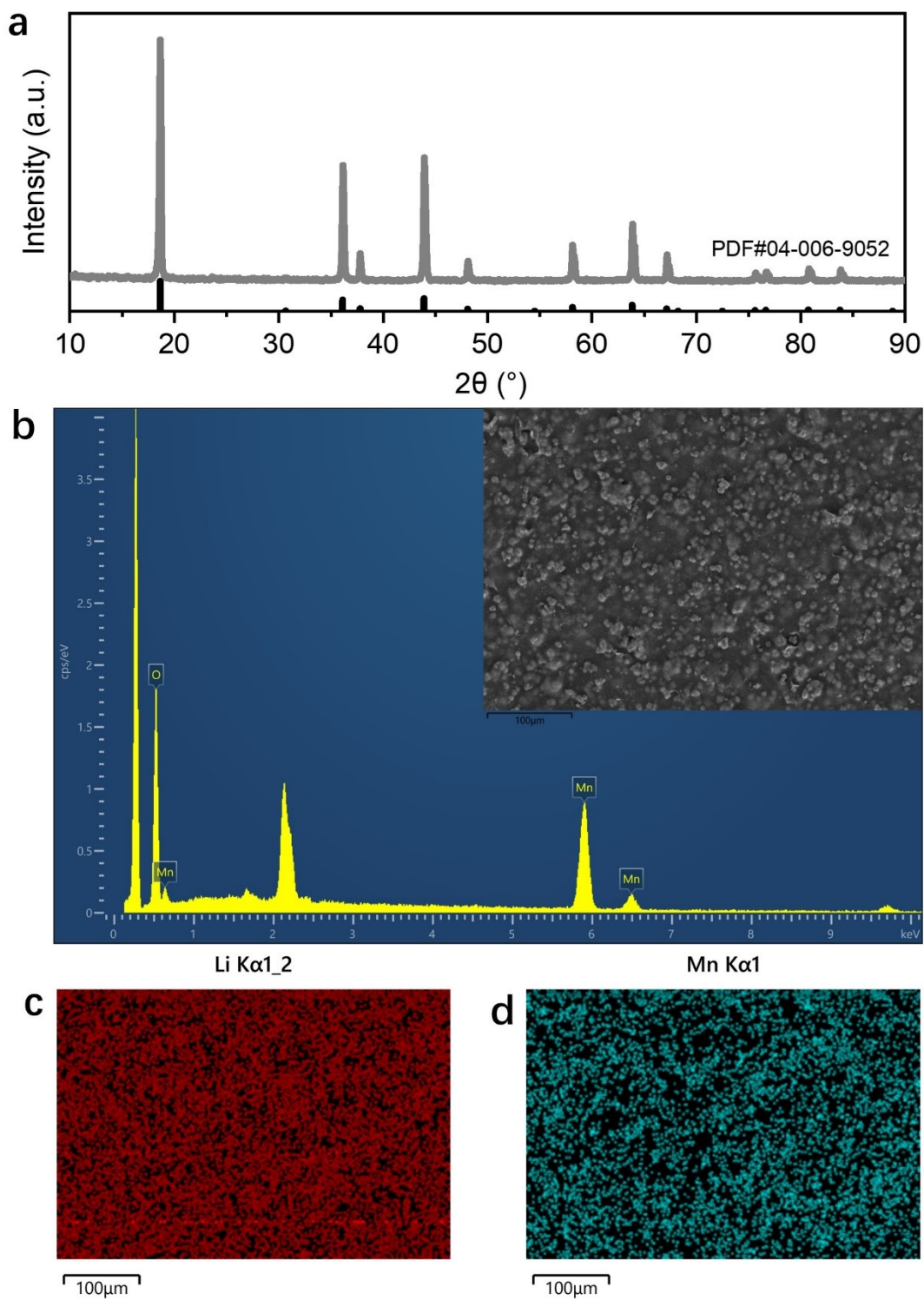


**Figure S19.** XRD pattern, SEM image, and EDS mapping images of LMO cathode used in this work.

**Table S1.** Fitting parameters for SAXS profiles in Figure 1c.

<b>Sample</b>	<b>A</b>	<b>B</b>	<b>C</b>	<b>n</b>	<b>r<sub>g</sub> (nm)</b>
<b>NC</b>	0.74	-2.48	0.29	2.36	3.19
<b>Swelled NC</b>	1.41	-24.28	0.63	2.25	10.14
<b>PC</b>	11.86	90.12	1.04	1.59	3.74
<b>Swelled PC</b>	9.05	59.42	1.15	1.87	4.04

**Table S2.** The comparison of the electrochemical strapping/plating cycles of Zn||Zn cells assembled by different cellulose-based separators.

<b>Samples</b>	<b>Current density (mA cm<sup>-2</sup>)</b>	<b>Cycles (N)</b>	<b>References</b>
Bacterial cellulose/ Ag Nanowires	2	2400	Adv. Mater. 2023, 35, 2304667
Sulfonated nanocellulose separator	2	1200	Adv. Funct. Mater. 2024, 34, 2315444.
Zr <sup>4+</sup> -hydrolysate-coated nanocellulose	1	1600	Adv. Funct. Mater. 2023, 33, 2304280.
Cotton-derived nanocellulose	1	2000	Energy Storage Mater. 2022, 44, 57-65.
Cellulose nanofibers- ZrO <sub>2</sub> composite	0.5	2000	Nano Energy 2021, 89, 106322.
Aero-bic bacteria nanocellulose	1	2800	Adv. Energy Mater. 2023, 13, 2302126.
Seaweed nanocellulose	1	1900	Chem. Eng. J. 2023, 466, 143312.
Hydrophilic bacterial cellulose	1	1200	Energy Storage Mater. 2025, 76, 104150.
Nanocellulose/ halloysite nanotubes	1	2500	Mater. Today Energy 2024, 46, 101736.
Bamboo nanocellulose	1	1000	Adv. Mater. 2024, 36, 2406429.
<b>PC (Nanocellulose/ polyoxometalate)</b>	<b>1</b>	<b>3000</b>	<b>This work</b>

## References

1. H. Yang, J. Edberg, V. Gueskine, M. Vagin, M. G. Say, J. Erlandsson, L. Wågberg, I. Engquist and M. Berggren, *Carbohydrate Polymers*, 2022, **278**, 118938.
2. S. Jin, J. Yin, X. Gao, A. Sharma, P. Chen, S. Hong, Q. Zhao, J. Zheng, Y. Deng and Y. L. Joo, *Nature communications*, 2022, **13**, 2283.
3. M. Kim, J. Lee, Y. Kim, Y. Park, H. Kim and J. W. Choi, *Journal of the American Chemical Society*, 2023, **145**, 15776-15787.